Covariance-Based MD Simulation Analysis Pinpoints Nanobody Attraction and Repulsion Sites on SARS-CoV-2 Omicron Spike Protein

Mert Golcuk[1], Fareeda E. Abu-Juam[1], Derman Basturk[2], Ayten Dilara Gursel[2], Clara Xazal Buran[2], Reyhan Metin Akkaya[2], Ahmet Yildiz[3,4], Mert Gur[1*]

[1] Department of Computational and Systems Biology, School of Medicine, University of Pittsburgh, Pittsburgh, PA, 15213, USA

[2] Department of Mechanical Engineering, Istanbul Technical University (ITU), 34437, Istanbul, Turkey

[3] Physics Department, University of California, Berkeley, CA, USA

[4] Department of Molecular and Cell Biology, University of California, Berkeley, CA, USA

*Corresponding Author: Mert Gur, gurmert@pitt.edu

Abstract

The heavily mutated receptor binding domain (RBD) of the SARS-CoV-2 Omicron Spike protein poses a challenge to the therapeutic efficacy of existing neutralizing antibodies and nanobodies. The molecular basis of their disrupted binding lies in the altered surface interactions between antibodies/nanobodies and the RBD. As such, we present a comprehensive all-atom molecular dynamics (MD) investigation of eleven distinct nanobodies (H11-H4, RE5D06, WNB2, MR17, Huo-H3, SB15, VHH-E, Ty1, NM1230, SB23, and SB45) bound to the Omicron spike RBD. Multi-microsecond all-atom MD simulations were combined with our recent practical covariance-based method analysis to map stabilizing vs. destabilizing interactions at the nanobody–RBD interfaces. This approach identified key residue contacts including hydrogen bonds, salt bridges, and hydrophobic interactions that stabilize each complex. Additionally, we identified charged repulsions and other unfavorable contacts introduced by Omicron mutations. Despite this diversity, certain RBD regions emerge as hotspots contacted by multiple nanobodies, while other interactions are unique to individual binders. Omicron-specific mutations are shown to disrupt or alter several nanobody contacts; in particular, our dynamic correlation analysis pinpoints cases of electrostatic clash (repulsive interactions) caused by residue substitutions in Omicron RBD. These destabilizing interactions correlate with reduced binding stability and help explain why some first-generation nanobodies lose efficacy against Omicron. Collectively, our results establish an integrated all atom MD and covariance analysis workflow that rapidly maps nanobody–RBD interfaces and quantifies how CDR sequence variations modulate binding energetics, insights that are critical for structure guided engineering. By pinpointing both stabilizing networks and mutation induced clash sites, the covariance method delivers a mechanistic blueprint for engineering next generation nanobodies capable of maintaining potency against ongoing SARS-CoV-2 evolution.

Introduction

Nanobodies (Nbs) are single-domain antibody (Ab) fragments (~12–15 kDa) derived from camelid heavy-chain Abs that offer unique advantages as therapeutics and diagnostics.[1, 2] Despite their small size, the three Nb complementarity-determining regions (CDR1–3) mediate specific and high affinity binding with target antigens. Their compact, monomeric structure with an elongated CDR3 loop enables Nbs to bind cryptic epitopes on target proteins that are often inaccessible to conventional antibodies.[3] In addition, Nbs exhibit high stability and affinity, comparable to full length antibodies, which are on average an order of magnitude larger than Nbs, making them powerful neutralizing agents in viral infections. Nbs' compact size, increased stability and ability to bind cryptic epitopes make them a useful candidate for targeting complexes such as SARS-CoV-2.

Since the emergence of SARS-CoV-2, numerous neutralizing nanobodies have been identified that target the spike (S) glycoprotein's RBD, blocking its interaction with the human angiotensin converting enzyme-2 (ACE2) receptor.[4] For example, nanobody H11-H4 can bind the receptor binding domain (RBD) without overlapping ACE2 and effectively displace ACE2 via electrostatic repulsion, whereas nanobody Ty1 binds the RBD at the ACE2 site (competing directly with the receptor).[4] Such mechanistic differences illustrate the diversity of how Nbs neutralize the virus, and they underscore the importance of mapping nanobody–RBD interactions in detail.

However, the SARS-CoV-2 has continued to evolve, accumulating a succession of mutations that enable new variants to evade existing Abs and prolong the pandemic. The Omicron lineage is particularly concerning as it carries an unusually large number of mutations, many clustered in the spike RBD. This domain is crucial for viral infectivity by mediating ACE2 binding and viral entry, and thus has been the principal target for vaccines, monoclonal Abs (mAbs), and Nbs.[5] Unfortunately, many mAbs and Nbs that were highly effective against the wild type (WT) strain have progressively lost potency with the emergence of the Omicron and Delta variants.[6] In fact, neutralizing effects of over 85% of tested RBD-targeted neutralizing antibodies were attenuated by the Omicron variant's mutations.[7] This caused the clinical efficacy of several Ab therapies to drop sharply and lead to the revocation of some emergency use therapeutic authorizations. These findings highlight that each new variant may require *new or optimized* Abs or Nbs and that rapid evaluation of binder antigen interactions is critical.

Conventional experimental screening alone cannot keep pace with the rate of SARS-CoV-2 antigenic drift. In this context, all-atom MD simulations have become a valuable tool to quickly assess how RBD mutations impact Ab/Nb binding at atomic resolution. MD simulations can capture the dynamic behavior of protein–protein interfaces and reveal changes in interaction networks and binding stability on nanosecond to microsecond timescales. Notably, our previous studies applied MD simulations to elucidate the binding mechanisms of nanobodies against earlier variants,[4] providing insight into how mutations (Alpha, Beta, and Delta variants) alter nanobody efficacy. Still, analyzing the massive amount of data from multi-microsecond MD trajectories is

challenging. Traditional approaches that enumerate all possible contacts or measure distances frame-by-frame become unwieldy when hundreds of residues interact at an interface; the nanobody H11-H4, for instance, involves roughly 78 interfacial residues when bound to Spike RBD. There is a pressing need for efficient computational pipelines that can automatically pinpoint the most relevant interactions (both favorable and unfavorable) from long MD simulations, thereby accelerating the design of countermeasures against immune-evading variants.

In this work, we address this need by performing extensive (>8 μs) physics-based all-atom molecular dynamics simulations to probe the binding poses and dynamics of multiple Nbs (H11-H4, RE5D06, WNB2, MR17, Huo-H3, SB15, VHH-E, Ty1, NM1230, SB23, and SB45)on the Omicron spike RBD, and then applying a recently developed covariance-matrix-based method to distill these trajectories into the key stabilizing and destabilizing contacts that govern each Nb-RBD interface. The simulations reveal that Omicron-specific point mutations remodel each Nb–RBD interface by shifting binding orientation, altering inter-domain dynamics, and rewiring hydrogen-bond, salt-bridge, and hydrophobic contact networks; atomic-level insights that serve as a blueprint for engineering next-generation Nbs with sustained potency against emerging SARS-CoV-2 variants.

Methodology

MD Simulations of Nanobody–Omicron RBD Complexes

We performed extensive all-atom MD simulations for each nanobody–RBD complex to characterize binding dynamics. Simulations were performed on the SARS-CoV-2 Omicron BA.5 S glycoprotein's RBD, which includes the array of mutations characteristic of this variant. Initial atomic coordinates for the RBD-Nanobody complexes were obtained by homology modeling based on known WT SARS-CoV-2 RBD-Nanobody complexes (Table 1). N-linked glycosylation at N343 on the RBD was included based on our previous studies. Each complex was placed in a cubic simulation box with a 25 Å padding of TIP3P explicit water model in all directions, ensuring ~50 Å separation between periodic images. The solvated system was neutralized, and ion concentration was set to 0.15 M NaCl. The final systems' sizes ranged from 120,000 to 150,000 atoms (Table 1).

The omicron RBD-Nanobody complexes were energy minimized for 10,000 steps to relieve steric clashes, followed by a multi-stage equilibration protocol. Initially, protein heavy atoms were restrained, and water and ion molecules were relaxed for 2 ns, then a second 10,000 steps of minimization was performed without any restraints. Further equilibration ensued for ~4 ns with harmonic restraints on C_α atoms, followed by an additional unrestrained equilibration of ~4 ns that allowed the complexes to fully adapt to the simulation conditions. Production MD simulations were run in the NPT ensemble using NAMD 3 with the CHARMM36 force field. Temperature was maintained at 310 K with a Langevin thermostat and pressure at 1 atm with a Langevin barostat, using a 2 fs time step. Long-range electrostatics were computed with the Particle Mesh Ewald (PME) method and a real-space cutoff of 12 Å for van der Waals interactions. Periodic

boundary conditions were applied in all dimensions. Each RBD–Nb system was simulated in two independent MD trajectories; each trajectory was 400 ns in length, yielding a total of 800 ns of simulation time per RBD–Nb type and 8.8 μs across all complexes. Coordinates were recorded every 50 ps.

Covariance-Based Interaction Mapping

To analyze the MD data, we employed the covariance-matrix based method[8, 9] that we developed to systematically identify important interprotein interaction hot spots. The core of this method is to compute residue-wise positional covariance (dynamic cross-correlation) matrices and extract RBD–nanobody residue pairs that move in a concerted fashion, indicative of direct or functionally relevant contact. This framework enables identification of attractive (stabilizing) and repulsive (destabilizing) interactions while avoiding an exhaustive scan of all possible residue pairs.

Our analysis proceeded as follows:

1. **Covariance Matrix Calculation:** For each RBD–Nb trajectory, the covariance (correlation) matrix between the positional fluctuations of all residue C_α atoms on the nanobody and those on the RBD were computed. This resulted in an $N_{nb} \times N_{RBD}$ matrix (where N_{nb} ~120 residues in the nanobody, N_{RBD} ~200 residues in RBD), in which each element *C(i,j)* represents the correlation of motions between nanobody residue *i* and RBD residue *j*. A positive *C(i,j)* (colored red in our maps) indicates that residues *i* and *j* tend to move in the same direction (highly correlated), often a signature of an attractive interaction holding them together. Conversely, a negative *C(i,j)* (blue) indicates anticorrelated motion, which can arise from repulsive interactions. The initial covariance matrix thus flags candidate contact pairs: strongly correlated pairs likely correspond to interface contacts that move as a unit, whereas strongly anticorrelated pairs may point to clashing residues that avoid each other.

2. **Spatial Filtering of Correlated Pairs:** Not all correlated motions correspond to direct interactions; some could be long-range allosteric correlations. We therefore applied a distance cutoff filter to focus on residue pairs that come into physical proximity. Any nanobody–RBD residue pair that interact within a threshold distance *d,* over the course of the simulation was discarded. We used ~11 Å for positively correlated pairs and ~13 Å for negatively correlated pairs, allowing a slightly longer range for repulsive effects. This yielded a "close-contact covariance matrix" emphasizing only those correlated pairs that are plausibly interacting at the interface. The spatial filter greatly reduces noise and spurious correlations, concentrating the analysis on the contact zone between the nanobody and RBD.

3. **Interaction Identification and Classification:** For each remaining correlated pair, we identified the specific type of interaction linking the two residues by examining their identities and relative geometries in the MD frames. Following established criteria, we

classified a pair as a stabilizing interaction if it consistently formed either a salt bridge (oppositely charged sidechains within ~6 Å), [10] a hydrogen bond (donor–acceptor ≤3.5 Å, angle ≥150°)[11] or a hydrophobic contact (nonpolar sidechains within ~8 Å)[12] during the simulation. In contrast, a correlated pair was classified as a repulsive interaction if the residues experienced like-charge electrostatic repulsion or other unfavorable contacts. Specifically, any instance of two positively charged groups (basic N atoms) or two negatively charged groups (acidic O atoms) coming within ≤12 Å was flagged as a same-charge repulsion, and any case of an aliphatic (hydrophobic) sidechain coming within ~12 Å of a charged residue was flagged as a hydrophobic–charged clash. These criteria are based on the recent covariance analysis methodology and efficiently capture destabilizing interactions that would not be identified by distance-only searches. By examining the MD frames where a given residue pair showed strong anticorrelation, we could confirm whether a specific like-charge encounter or unfavorable contact was indeed occurring (supporting its classification as a repulsive interaction).

4. **Mapping Interaction Frequencies:** Finally, we quantified how prevalent each identified interaction was throughout the simulations. For every residue pair identified in step 3, we calculated the interaction frequency; the percentage of simulation frames in which that pair was found to be in contact (for attractive interactions) or in a repulsive configuration. This yields an interaction frequency map for each nanobody–RBD complex, analogous in format to the covariance map but with color intensity representing % occupancy rather than correlation. In our visualization, we plot attractive contact frequencies on a red scale (0 to 100% in red hues) and repulsive interaction frequencies on a blue scale (0 to -100% in blue hues). This dual-color scheme conveniently captures the balance of favorable vs. unfavorable interactions: a deep red spot signifies a contact present nearly constantly (highly stabilizing), whereas a deep blue spot indicates a persistently recurring repulsion or clash at that residue pair. Pairs that are rarely in contact appear light or white (near 0%). By compiling these maps, we can directly compare how each Nb engages the RBD, which residues form frequent bonds, and whether any mutations introduce consistently repelling contacts.

All analysis steps were carried out using custom MATLAB scripts in combination with VMD for trajectory processing. The covariance matrices were computed from concatenated trajectories of each Nb–RBD (after aligning on the RBD to focus on interface motion). We emphasize that this pipeline dramatically reduces the data to a manageable set of key interactions. Instead of manually sifting through thousands of frame-by-frame contacts, the correlation analysis automatically highlights the "important" residue pairs that define binding. The methodology has previously[9] captured known interactions in Nb–Spike complexes and even identified unexpected repulsive interactions introduced by variant mutations. For example, in an earlier study of H11-H4, this approach revealed that the Beta variant's E484K mutation broke a stabilizing salt bridge and

replaced it with a charge–charge repulsion between RBD and nanobody residues. We leverage the same approach here to decode the Omicron variant's effects on a broad panel of nanobodies.

Results and Discussion

Normalized $C_\alpha - C_\alpha$ covariance matrices were calculated for every Omicron RBD–Nb complex. After applying a spatial filter that retained only residue pairs falling within interaction distance, we obtained close-contact covariance matrices that act as dynamic fingerprints of each interface. In these two-dimensional maps, red regions correspond to residue pairs whose movements are positively correlated; i.e., they attract one another and stabilize binding, whereas blue regions highlight residue pairs that move in opposite directions and therefore experience repulsive interactions that induce strain on binding and have destabilizing effect. The overall pattern immediately reveals that seven Nbs (H11-H4, RE5D06, WNB2, MR17, Huo-H3, SB15 and VHH-E) bind almost exclusively along the receptor-binding ridge of the RBD (residues 440–510), while Ty1, NM1230, SB23 and SB45 span the ridge but also involve portions of the N-terminal RBD core (residues 340–355). These distinct binding footprints manifest as markedly different clusters of correlated residues along the RBD axis.

To quantify the balance between favorable and unfavorable couplings, we defined an *interaction score* as the sum of all Nb–RBD covariance elements. Higher positive scores mark complexes in which attractive interactions outweigh repulsions, while lower positive and negative scores identify interfaces in which Omicron mutations have introduced recurring clashes that erode stability.

Correlation analysis (Figure 1A) indicates specific patterns for each nanobody. H11-H4 positively correlated with RBD residues 349–353, 447–457, 469–473, and 488–496, while negatively correlated with residues 479–487, resulting in an interaction score of 2579.5. RE5D06 showed positive correlations with residues 446–457 and 484–497, and negative correlations with residues 468–471 and 482–489, yielding an interaction score of 2535.3. WNB2 displayed strong positive correlations across residues 443–457 and 482–502, with negative correlation limited to residue 482, culminating in an interaction score of 5095.7. MR17 exhibited positive correlations with residues 445–453 and 472–498, but negative correlations with residues 490–505, leading to an interaction score of 4846.3. Huo-H3 presented positive correlations at residues 447–449, 468–473, and 489–496, counterbalanced by negative correlations at residues 452–453 and 480–487, giving a negative interaction score of -471.8. Similarly, SB15, with positive correlations at residues 415–421, 453–456, and 485–493, was heavily impacted by negative correlations spanning residues 486–506, resulting in an interaction score of -252.9. VHH-E, by contrast, demonstrated positive correlations with residues 443–449, 475–478, and 484–503, achieving an interaction score of 3522.3.

For Nbs with broader interactions (Figure 1B), Ty1 exhibited positive correlations with residues 349–353, 444–453, 468–472, and 481–496, achieving an interaction score of 4193.2. SB45 showed positive correlations with residues 447–455, 468–472, and 481–497 but negative

correlations at residues 417 and 455, resulting in a score of 2472.1. NM1230 was positively correlated with residues 348–354, 446–472, 465–471, and 488–497, and negatively correlated with residues 482–487, yielding an interaction score of 2318.2. SB23 exhibited positive correlations with residues 344–350, 440–453, and 491–500, balanced by negative correlations at residues 468–471 and 482–489, giving an interaction score of 2546.6.

Further analysis (Figure 2) identified specific attractive and repulsive interactions based on defined physical criteria. Attractive interactions included hydrogen bonds (donor–acceptor ≤ 3.5 Å, angle $\geq 150°$), salt bridges (≤ 6 Å), and hydrophobic contacts (≤ 8 Å), while repulsive interactions involved like-charge or hydrophobic-charged clashes within 12 Å. H11-H4 exhibited attractive interactions (Hydrophobic interactions and hydrogen bonds) with residues 449–457 and 489–497, and repulsive interactions (Aliphatic-polar) with residues 483–484. RE5D06 formed attractive contacts (Hydrophobic interactions, salt-bridge, and hydrogen bonds) with residues 449–456, 472–475, and 483–494. WNB2 had extensive attractive interactions (Hydrophobic interactions, salt-bridge, and hydrogen bonds) with residues 446–456, 483–494, and 498–501, but repulsive interaction (Aliphatic-polar) at residue 480. MR17's attractive interactions (Hydrophobic interactions, salt-bridge, and hydrogen bonds) occurred between residues 449 and 478–495, with repulsive interactions (Aliphatic-polar) at residues 442, 492, and 498. Huo-H3 displayed attractive interactions (Hydrophobic interactions) at residues 449, 483–491, and 496, but strong repulsive interactions (Aliphatic-polar and charge-charge repulsion) at residues 452–455, 480–485, and 493. SB15 showed attractive contacts (Hydrophobic interactions) at residues 445, 455–456, 475, 486, 493–495, and 503, yet encountered repulsive interactions (Aliphatic-polar) at residues 445, 483, and 498. VHH-E engaged attractively (Hydrophobic interactions, salt-bridge, and hydrogen bonds) with residues 444–452, 478, and 484–492. Ty1 established attractive interactions (Hydrophobic interactions and hydrogen bonds) at residues 352, 447–452, and 482–490. NM1230 engaged attractively (Hydrophobic interactions, salt-bridge, and hydrogen bonds) at residues 348–352, 445–451, 468–470, and 490–495, but faced repulsive interactions (Aliphatic-polar) at residues 346 and 484. SB23 had attractive contacts (Hydrophobic interactions, salt-bridge, and hydrogen bonds) with residues 445–450 and 490–492, balanced by repulsive interactions (Aliphatic-polar) at residues 483–484. Finally, SB45 interacted positively (Hydrophobic interactions, salt-bridge, and hydrogen bonds) with residues 449, 452, 471, 483–484, and 491–494, but experienced repulsive interactions (Aliphatic-polar) at residue 455.

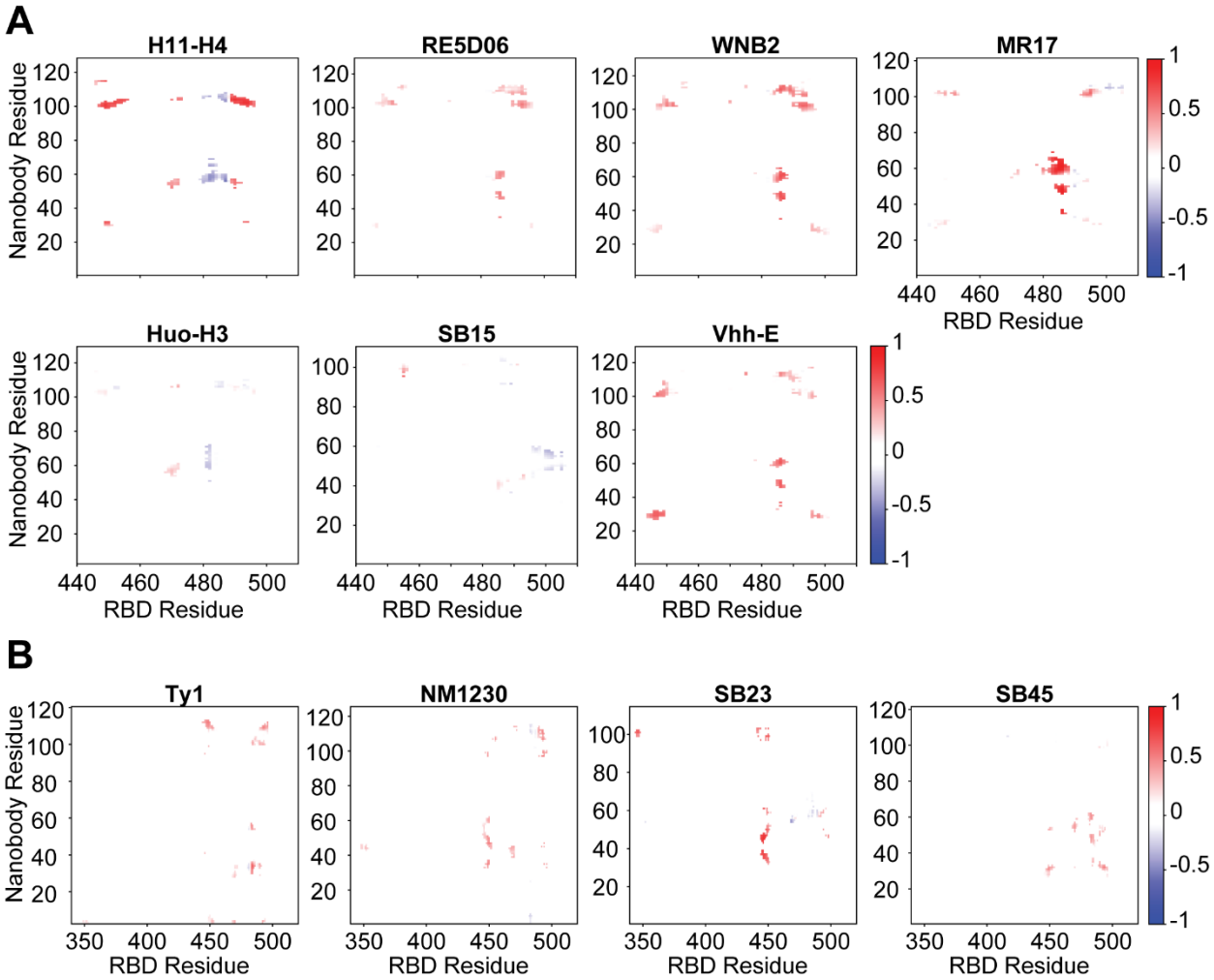

Figure 1. Covariance for nanobody–Omicron RBD complexes. *(A) Nanobodies H11-H4, RE5D06, WNB2, MR17, Huo-H3, SB15, VHH-E; (B) Nanobodies Ty1, NM1230, SB23, SB45. Each panel is a matrix mapping residue–residue correlation between the nanobody (y-axis, residue index) and the Omicron BA.5 RBD (x-axis, residue index). Red shading indicates positively correlated motions corresponding to attractive (stabilizing) interactions, while blue indicates negatively correlated (repulsive) motions corresponding to repulsive (destabilizing) interactions. Only residue pairs that come within contact range are shown (distant pairs filtered out).*

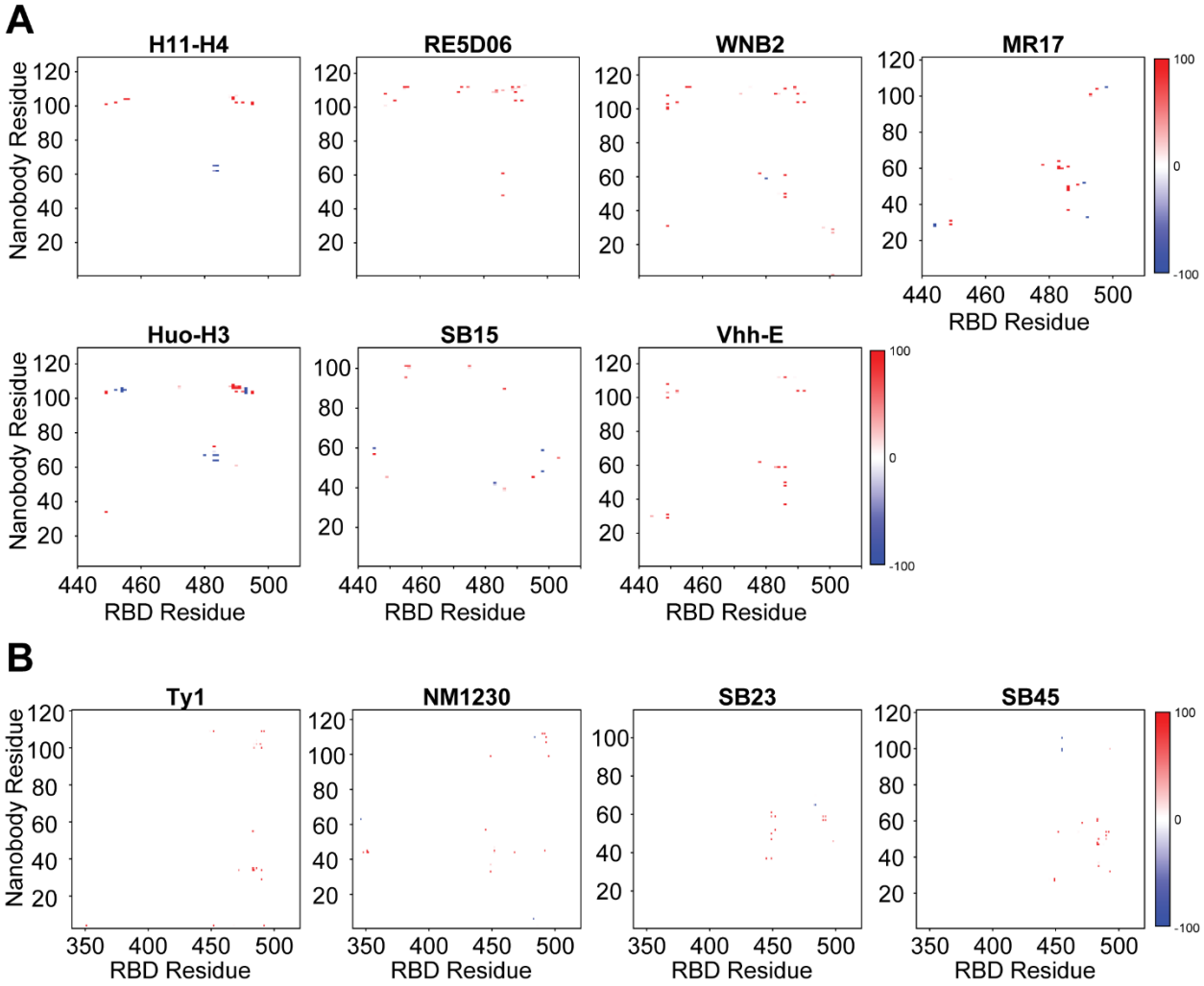

Figure 2. Interaction frequency for nanobody–Omicron RBD complexes. *(A) Nanobodies H11-H4, RE5D06, WNB2, MR17, Huo-H3, SB15, VHH-E; (B) Nanobodies Ty1, NM1230, SB23, SB45. These graphs show the percentage of simulation frames in which a given nanobody residue–RBD residue pair is interacting. The color scale (right) ranges from 0 (white) to +100% (red) for attractive interactions, and 0 to –100% (blue) for repulsive interactions.*

Conclusion

We have performed all-atom MD simulations and subsequent in-depth covariance-based correlation and interaction analyses of eleven Nbs bound to the SARS-CoV-2 Omicron variant's RBD, yielding a detailed picture of both stabilizing and destabilizing interactions at these antibody–antigen interfaces. The study highlights how Omicron's constellation of RBD mutations reshapes interfacial interaction networks: while core binding epitopes remain intact for some broadly neutralizing Nbs, others lose key contacts or acquire new electrostatic clashes that weaken affinity. By mapping dynamic residue correlations, we identified the critical contacts (salt bridges, hydrogen bonds, and hydrophobic interactions) that each Nb relies on, and we pinpointed

vulnerability hotspots, which are specific residue pairs where Omicron substitutions introduce strain or repulsion.

Our findings underscore several broad principles. First, Nb binding footprints are diverse; a mutation that knocks out one Nb is not guaranteed to affect another, which is encouraging for combination therapies**.** Second, certain RBD regions (e.g., the ACE2-binding site) are frequent targets of Nbs and thus frequent targets of viral escape; future Nb designs should consider focusing on more conserved surfaces or incorporate adaptability at those key positions. Third, the covariance-based method proves to be a powerful tool for rapid, high-resolution analysis of protein–protein interactions in large datasets of simulations, distilling complex motions into intuitive color-coded maps of interactions. In practical terms, this approach greatly accelerates the iterative optimization of Nbs: one can quickly simulate a candidate, see which interactions are suboptimal, tweak the design, and repeat , all in silico, before moving to laborious wet-lab assays.

For the Omicron RBD and the Nbs studied, our analysis suggests specific pathways to improvement. Nbs like H11-H4 and Ty1, which lost efficacy against Omicron, could regain potency through structure-guided mutations that restore complementarity. Nbs like NM1230 and MR17 that retained strong interactions serve as a baseline for what designs work across variants.

The methodology and results herein provide a framework for fast-tracking Nb evaluation against SARS-CoV-2 variants. As new variants (or entirely new pathogens) emerge, such computational pipelines will be invaluable for staying ahead in the arms race of antigenic evolution versus therapeutic design. We anticipate that the insights gained will aid in the rational design of variant-proof nanobodies and inspire further integration of MD simulation data into the development cycle of biologics.

References

1. Bannas, P., Hambach, J. & Koch-Nolte, F. Nanobodies and Nanobody-Based Human Heavy Chain Antibodies As Antitumor Therapeutics. *Front Immunol* **8**, 1603 (2017).
2. Jin, B.K., Odongo, S., Radwanska, M. & Magez, S. NANOBODIES®: A Review of Diagnostic and Therapeutic Applications. *Int J Mol Sci* **24** (2023).
3. Zhu, H. & Ding, Y. Nanobodies: From Discovery to AI-Driven Design. *Biology (Basel)* **14** (2025).
4. Golcuk, M., Hacisuleyman, A., Erman, B., Yildiz, A. & Gur, M. Binding Mechanism of Neutralizing Nanobodies Targeting SARS-CoV-2 Spike Glycoprotein. *J Chem Inf Model* **61**, 5152-5160 (2021).
5. Schoof, M. et al. An ultrapotent synthetic nanobody neutralizes SARS-CoV-2 by stabilizing inactive Spike. *Science* **370**, 1473-1479 (2020).
6. Liu, B. et al. Enhanced potency of an IgM-like nanobody targeting conserved epitope in SARS-CoV-2 spike N-terminal domain. *Signal Transduct Target Ther* **9**, 131 (2024).
7. Cao, Y. et al. Omicron escapes the majority of existing SARS-CoV-2 neutralizing antibodies. *Nature* **602**, 657-663 (2022).
8. Gur, M. & Erman, B. Quasi-harmonic fluctuations of two bound peptides. *Proteins* **80**, 2769-2779 (2012).
9. Golcuk, M. & Gur, M. A Practical Covariance-Based Method for Efficient Detection of Protein-Protein Attractive and Repulsive Interactions in Molecular Dynamics Simulations. *bioRxiv*, 2025.2003.2024.644990 (2025).
10. Beckstein, O., Denning, E.J., Perilla, J.R. & Woolf, T.B. Zipping and unzipping of adenylate kinase: atomistic insights into the ensemble of open<-->closed transitions. *J Mol Biol* **394**, 160-176 (2009).
11. Durrant, J.D. & McCammon, J.A. HBonanza: a computer algorithm for molecular-dynamics-trajectory hydrogen-bond analysis. *J Mol Graph Model* **31**, 5-9 (2011).
12. Stock, P., Utzig, T. & Valtiner, M. Direct and quantitative AFM measurements of the concentration and temperature dependence of the hydrophobic force law at nanoscopic contacts. *J Colloid Interface Sci* **446**, 244-251 (2015).

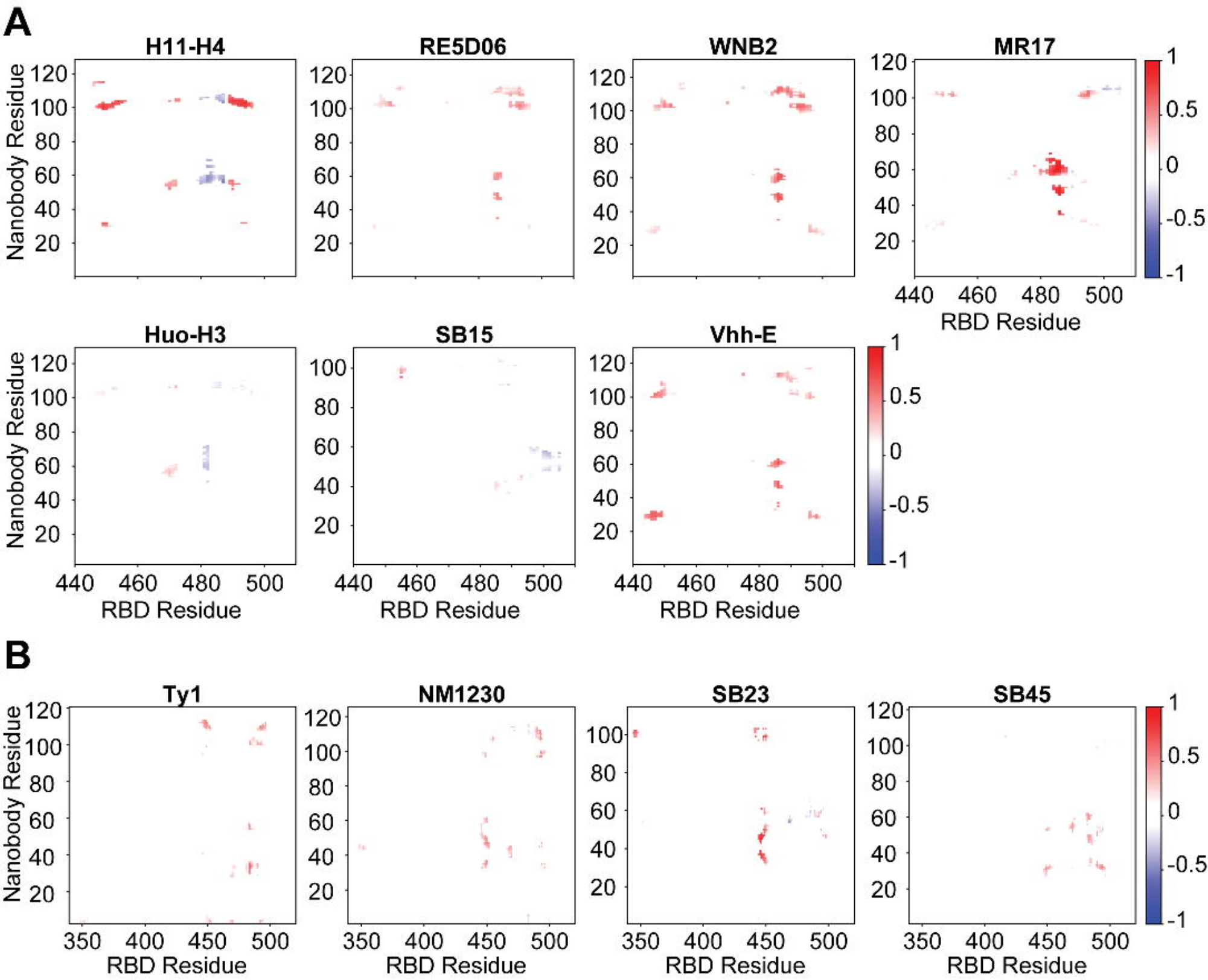
A
H11-H4
RE5D06
WNB2
MR17
Huo-H3
SB15
Vhh-E
Nanobody Residue
RBD Residue
B
Ty1
NM1230
SB23
SB45
Nanobody Residue
RBD Residue

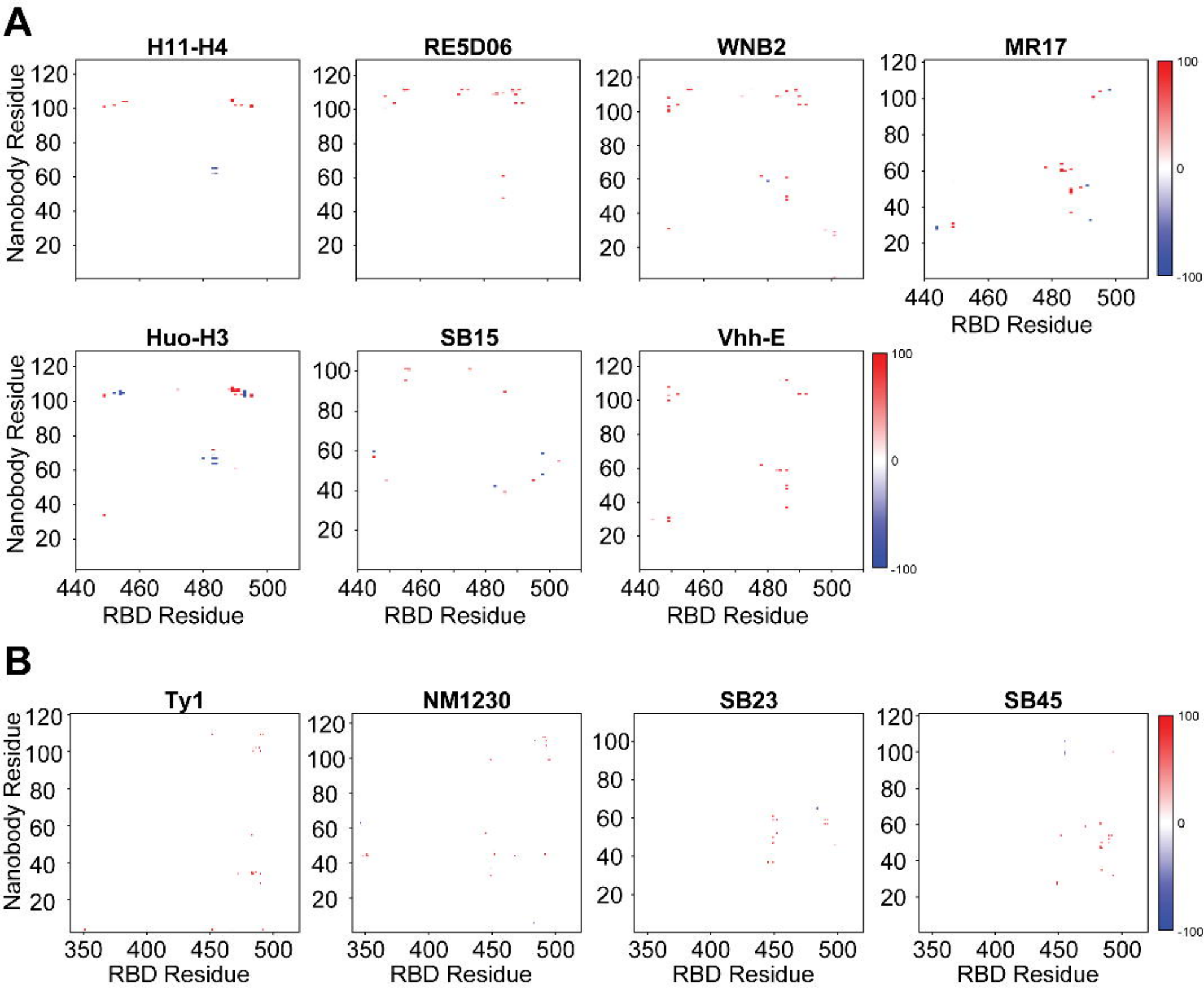
A
H11-H4
RE5D06
WNB2
MR17
Huo-H3
SB15
Vhh-E
Nanobody Residue
RBD Residue
B
Ty1
NM1230
SB23
SB45
Nanobody Residue
RBD Residue